JOURNAL OF SPACECRAFT AND ROCKETS
Vol. 46, No. 2, March–April 2009

Analytical Model for Cryogenic Stratification in a Rotating and Reduced-Gravity Environment

Justin Oliveira* and Daniel R. Kirk†
Florida Institute of Technology, Melbourne, Florida 32901
and
Paul A. Schallhorn‡
NASA Kennedy Space Center, Florida 32899

DOI: 10.2514/1.39760

Modeling the thermal behavior of cryogenic propellants within the upper stages of a launch vehicle is necessary for successful mission planning. During orbital transfer, the upper stage may coast for several hours, during which the propellants are heated by solar radiation and undergo thermal stratification. At the end of a coast, the propellant temperature and pressure must be within a narrowly defined range to ensure engine restart. This work develops a thermal stratification model that includes the thermal conditioning spin of the stage. The model may be used to assess the impact of thermal stratification within propellant tanks over a range of axial accelerations, spin rates, heat fluxes, and tank geometries. The parabolic dishing effect from spinning the tank results in an increased stratum thickness, due to the larger length of the free-convection boundary layer along the tank wall. However, due to the balance between the increased wall-heating area and increased free-surface area, stratum temperatures may be cooler or warmer, depending on the spin rate.

Nomenclature

c_p	=	specific heat at constant pressure, J/kg · K
Gr	=	Grashof number
g	=	acceleration, m/s^2
H	=	initial bulk liquid fill level, m
h	=	convective heat transfer coefficient, W/m^2 · K
h	=	height of paraboloid surface of revolution, m
L	=	tank height, m
$\dot{m}$	=	mass flow, kg/s
Nu	=	Nusselt number
P	=	pressure, N/m^2
Pr	=	Prandtl number
q''	=	heat flux, W/m^2
R	=	tank radius, m
Ra	=	Rayleigh number
S_p	=	surface area of liquid-ullage interface, m^2
T	=	temperature, K
t	=	time, s
x, y	=	length, m
β	=	volumetric thermal expansion coefficient, K^{-1}
Δ	=	thickness of the stratified layer, m
δ	=	boundary-layer thickness, m
θ	=	temperature difference, K
κ	=	thermal conductivity, W/m K
μ	=	dynamic viscosity, N · s/m^2
ν	=	kinematic viscosity, m^2/s
ρ	=	density, kg/m^3
ω	=	spacecraft rotational spin rate, deg /s

Subscripts

b, 1	=	bulk fluid
bl	=	boundary layer
d	=	diffusion
g	=	gas
i	=	interface or initial
l	=	liquid
m	=	mixed
s, 2	=	stratum
u, 3	=	ullage gas
w	=	wall
0	=	reference

I. Introduction

PREDICTION of propellant behavior in launch vehicle upper stages is necessary for successful mission planning [1,2]. During orbital transfer (e.g., low Earth orbit to geostationary Earth orbit), the upper-stage nominally coasts with a low-acceleration settling thrust and is spun about its longitudinal axis for thermal conditioning. Solar heating during transfer thermally stratifies the cryogenic propellants, and if the propellants are outside of a specified temperature and pressure range, the engine may not restart at insertion. The purpose of this work is to develop an improved analytical model of thermal stratification that captures the influence of reduced-gravity (low axial acceleration) and rotating environments, both of which are important for propellant thermodynamic modeling in upper-stage vehicles. The development of this model is significant, in that prior stratification models do not have the capability to handle boundary-layer transition or the effects of tank rotation, rendering them inappropriate for thermal analysis of the propellant within the tanks of launch vehicle upper stages. First, this work reviews prior analytical stratification models and makes several modifications for handling low-gravity scenarios in which boundary-layer transition commonly occurs. Second, a new stratification model that accounts for the behavior of the liquid propellant under rotation is developed. Finally, the models are applied to several candidate scenarios that are typical of the coast phases. Although the model does not capture all details of the flowfield, it can be used as a rapid scoping tool to explore a variety of scenarios and is more computationally efficient than computational fluid dynamics (CFD) solutions.

Presented as Paper 5059 at the 2006 AIAA Joint Propulsion Conference, Sacramento, CA, 9–12 August 2006; received 14 July 2008; revision received 30 September 2008; accepted for publication 7 October 2008.

*Graduate Research Assistant, Mechanical and Aerospace Engineering Department. Member AIAA.
†Assistant Professor, Mechanical and Aerospace Engineering Department. Senior Member AIAA.
‡Head, Environments and Launch Approval Branch. Senior Member AIAA.

II. Thermal Stratification Analytical Modeling

The principal mechanism by which mass and energy are transported within the tank is buoyancy-induced natural convection, which is initiated by solar heating of the tank. A free-convection boundary layer forms due to the lower density of the warm fluid along the walls of the tank. Mass is entrained into the boundary layer, heated, and transported to the upper region of the cold bulk fluid, forming a thermally stratified layer. If this layer of fluid propagates to the entrance of the turbomachinery and is warmer than a specified value, the turbopump may not function properly. Figure 1 shows the nomenclature of the model used to predict the growth of the stratified layer, $\Delta(t)$, and the temperature of the stratum layer, T_s, within a smooth-walled cylindrical tank.

Figure 2 shows the parabolic dishing effect of the liquid due to the thermal conditioning spin about the longitudinal axis of the tank. In Fig. 2, the tank radius R is 3 m, the spin rate ω is 1 deg/s, and the axial acceleration of the tank or reduced-gravity ratio g/g_0 is 10^{-4}. This work develops analytical models to predict the stratified thermodynamic state of fluids over a range of conditions for cryogenic hydrogen and oxygen, including the effect of spinning the tank. The parameters used in this study are summarized in Table 1.

A. Governing Nondimensional Numbers

The primary parameter used to classify flows of this type is the Rayleigh number Ra, which is a product of the Grashof number Gr (ratio of buoyancy to viscous forces) and Prandtl number Pr (ratio of viscous to thermal diffusivity). Equation (1) gives the Rayleigh number for buoyancy-driven flows with constant wall temperature T_w:

$$Ra = Gr\,Pr = \frac{g\beta\theta_w x^3}{\nu^2}\,\frac{\mu c_p}{\kappa} \tag{1}$$

where μ is the dynamic viscosity, ν is the kinematic viscosity, c_p is the specific heat, k is the thermal conductivity, β is the liquid expansion coefficient, g is the local axial acceleration, θ_w is the temperature difference between the wall temperature T_w and the bulk-fluid temperature T_b, and x is a vertical coordinate measured from the origin of the boundary layer. The boundary-layer transitions from laminar to turbulent around $Ra \sim 10^9$ and Eq. (1) may be solved for the transition distance. Equation (2) gives a modified Rayleigh number $Ra*$ for buoyant flows driven by uniform heat flux, and the transition Rayleigh number is around $Ra^* \sim 10^{11}$:

$$Ra^* = Gr^*\,Pr = \frac{g\beta q''_w x^4}{k\nu^2}\,\frac{\mu c_p}{\kappa} \tag{2}$$

For a cylindrical tank with $L = 2R = 3$ m and a fill level of $H = 0.6$ m (20% of L), Eq. (2) predicts that for heat fluxes below 100 W/m^2 and axial accelerations below 10^{-4} g/g_0, the free-convection boundary layer that forms along the inside walls of the tank is laminar. This is in contrast to propellant stratification situations that arise when the vehicle is on the launch pad ($g/g_0 = 1$), where both Ra and $Ra*$ are orders of magnitude above transition and the free-convection boundary layer on the inside of the tank walls is turbulent [1]. The nature of this boundary layer is important to determine the rate of the thermal stratification as well as the final stratum temperature.

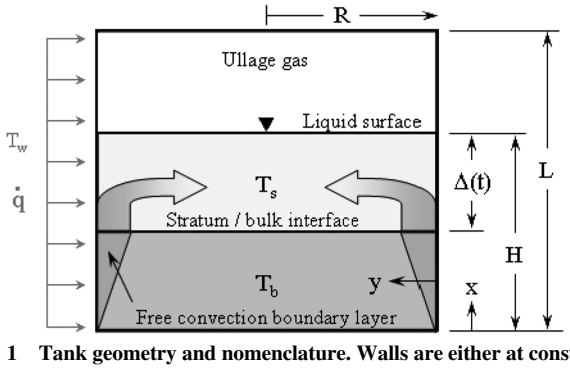

Fig. 1 Tank geometry and nomenclature. Walls are either at constant temperature or constant heat flux.

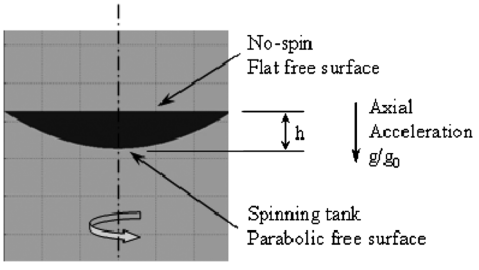

Fig. 2 Parabolic dishing effect due to spacecraft spinning about the longitudinal axis.

Table 1 Modeling parameters for cryogenic LH_2 and LOX

Parameter	Range of investigation
Ullage pressure	$140 < P < 280$ kPa
Ullage pressurants	Hydrogen tank: GH_2 Oxygen tank: O_2 and He
Bulk propellant temperature T_b	$15\text{ K} \le T_{b,LH_2} \le 20\text{ K}$ $90\text{ K} \le T_{b,LOX} \le 110\text{ K}$
Driving temperature difference $\theta_w = T_w - T_b$	$0.1\text{ K} \le \theta_w \le 5\text{ K}$
Wall heat fluxes q''_w	$5 \le q''_w \le 100$ W/m^2
Axial acceleration or reduced-gravity ratio g/g_0	$10^{-5} \le g/g_0 \le 1$
Spin rate ω	$0.1\text{ deg/s} \le \omega \le 10\text{ deg/s}$
Initial tank fill height H	$10\% \le H \le 50\%$ of L
Coast duration	1–4 h

B. Constant-Wall-Temperature Analysis

The growth of the stratified layer is governed by the rate at which boundary-layer mass flow crosses the interface between the bottom of the stratum and the top of the cold bulk-fluid layer. The interface is located at $H - \Delta(t)$ as measured from the bottom of the tank, as shown in Fig. 1. The boundary-layer mass flow is given by Eq. (3), where ρ is the liquid density, $u(y)$ is the local radially dependent vertical velocity profile in the boundary layer, and δ is the boundary-layer thickness:

$$\dot{m}_{\text{bl}} = 2\pi R\rho \int_0^{\delta} u(y)\mathrm{d}y \tag{3}$$

Velocity and temperature profiles within a laminar boundary layer are given by Eqs. (4) and (6) [3].

Laminar:

$$u(y) = u_0 \frac{y}{\delta}\left(1 - \frac{y}{\delta}\right)^2 \tag{4}$$

Laminar:

$$u_0 = 5.17\nu x^{1/2}\left[\frac{20}{21} + \frac{1}{Pr}\right]^{-1/2}(Gr)^{1/2} \tag{5}$$

Laminar:

$$\theta(y) = \theta_w\left(1 - \frac{y}{\delta}\right)^2 \tag{6}$$

where $\theta(y) = T(y) - T_b$ and $\theta_w = T_w - T_b$, where T_w is the wall temperature, and T_b is the bulk-fluid temperature. Depending on heating and axial acceleration levels, the boundary layer may be turbulent, and many models rely on the results of the turbulent free-convection boundary layer at constant wall temperature, as analyzed by Eckert and Jackson [3]. The velocity and temperature profiles

within a turbulent boundary layer are given by Eqs. (7) and (9), respectively.

Turbulent:

$$u(y) = u_1\left(\frac{y}{\delta}\right)^{1/7}\left(1-\frac{y}{\delta}\right)^4 \tag{7}$$

Turbulent:

$$u_1 = 1.185\frac{\nu}{x}(Gr)^{1/2}[1+0.49(Pr)^{2/3}]^{-1/2} \tag{8}$$

Turbulent:

$$\theta(y) = \theta_w\left[1-\left(\frac{y}{\delta}\right)^{1/7}\right] \tag{9}$$

Assuming constant properties, Bailey et al. [4] apply an energy balance between the heat entering the tank below the stratum, $H-\Delta(t)$, and the heated mass flow exiting the boundary layer at the stratum interface:

$$q''(H-\Delta) = h\theta_w(H-\Delta) = c_p\rho\int_0^\delta \theta(y)u(y)\mathrm{d}y \tag{10}$$

Combining Eqs. (3) and (10) yields an expression for the boundary-layer mass flow at the bulk-fluid-stratified fluid datum: Eq. (11). The analogous expression for the case of a turbulent boundary layer is given in Eq. (12).

Laminar:

$$\dot{m}_{\mathrm{bl}} = \pi R^2\rho\left(\frac{d\Delta}{dt}\right) = \frac{5\pi hR}{c_p}(H-\Delta) \tag{11}$$

Turbulent:

$$\dot{m}_{\mathrm{bl}} = \pi R^2\rho\left(\frac{d\Delta}{dt}\right) = \frac{8\pi hR}{c_p}(H-\Delta) \tag{12}$$

Equations (11) and (12) assume that as the mass flow exits the boundary layer it instantaneously forms a uniform thickness disk of the stratified fluid above the bulk. However, at low axial acceleration levels it may take a substantial amount of time for the warm boundary-layer flow to travel to the center of the tank to form the initial stratified layer [5]. The radial flow component of the warm fluid exiting the boundary layer into the stratum is not considered in the model. Furthermore, the secondary recalculating flow that develops as the warm stratum is forced back down the centerline of the tank, and subsequently cooled by the bulk fluid, is also neglected.

Integrating Eqs. (11) and (12) and recognizing that the heat transfer coefficient h must be evaluated at the vertical location corresponding to the bottom of the stratum $[H-\Delta(t)]$, which varies with time, yields expressions for the growth of the stratum layer, $\Delta(t)$, for laminar [Eq. (13)] and turbulent free-convection boundary layers [Eq. (14)].

Laminar:

$$\frac{\Delta(t)}{H} = 1-e^{\frac{-5ht}{Rc_p\rho}} \tag{13}$$

Turbulent:

$$\frac{\Delta(t)}{H} = 1-e^{\frac{-8ht}{Rc_p\rho}} \tag{14}$$

For the case of constant wall temperature, the convective heat transfer coefficient is evaluated using curve fits for either laminar or turbulent boundary layers, given by Eckert and Jackson [3].

Laminar:

$$Nu_{\mathrm{av}} = 0.555(Gr\,Pr)^{1/4} \tag{15}$$

Turbulent:

$$Nu_{\mathrm{av}} = 0.0210(Gr\,Pr)^{2/5} \tag{16}$$

With the stratum growing with time, the heat transfer coefficient varies because the Grashof number is reduced as the boundary-layer run length $x = H-\Delta(t)$ decreases. This means that in Eqs. (13) and (14), the heat transfer coefficient must be evaluated at the location of the stratum-fluid/bulk-fluid interface. Equations (15) and (16) apply to boundary layers developing over smooth vertical plates. Although the liquid-oxygen tank contains a smooth wall, the internal surfaces of the liquid-hydrogen tank usually have mass-saving isogrid, and the nature of the boundary layer is not similar to predictions for smooth flat plates [6]. Wall curvature is also neglected in the models.

To find the stratum temperature, a second energy balance is applied in which the heat entering the fluid through the tank walls, $2\pi RH$, goes into heating the stratum volume, $\pi R^2\Delta$. The energy balance can be written as in Eq. (17):

$$q''2\pi RH = h\theta_w 2\pi RH = \rho\pi R^2\Delta c_p\frac{d\theta_s}{dt} \tag{17}$$

In Eq. (17), the heat flux is rewritten in terms of a product of heat transfer coefficient and temperature difference and neglects any energy interaction with the ullage gas. Equation (17) may be integrated to find the stratum temperature:

$$T_s = (\theta_w+T_b) - \theta_w e^{\frac{-2Hht}{R\Delta c_p\rho}} \tag{18}$$

In Eq. (17), it is assumed that the product of heat transfer coefficient and temperature difference is the same adjacent to both the bulk fluid and the stratum layer. In actuality, the heat transfer coefficient is different in the stratum and bulk layers. To improve the model, the heat transfer coefficient was taken to vary between the bulk and stratum layers; coefficients for both layers are found by performing an average within the separate regions. Equation (17) may also be rewritten including the addition of a term for stratum-ullage interaction (diffusion and energy exchange, of which some goes into heating the stratum layer, whereas the remainder causes phase change):

$$h_1\theta_w 2\pi R(H-\Delta) + h_2\theta_s 2\pi R\Delta + \pi R^2 q_d'' = \rho\pi R^2\Delta c_p\frac{d\theta_s}{dt} \tag{19}$$

Equation (19) can be integrated to find the stratum temperature, where h_1 and h_2 are the heat transfer coefficients for the bulk region and stratum region, respectively:

$$T_s = \frac{(H-\Delta)}{\Delta}\frac{h_1}{h_2}\theta_w + \frac{Rq_d''}{2h_2\Delta} - \frac{2(H-\Delta)h_1\theta_w + Rq_d'' + 2h_2\theta_w\Delta}{2h_2\Delta}e^{\left(\frac{-2h_2}{Rc_p}\right)} + (\theta_w+T_b) \tag{20}$$

Ullage temperature is found independently using an energy balance:

$$q''2\pi R(L-H) = h_3\theta_u 2\pi R(L-H) = \rho\pi R^2(L-H)c_p\frac{d\theta_u}{dt} \tag{21}$$

Equation (21) can be integrated to find the ullage temperature, where h_3 is the heat transfer coefficient for the ullage region, and $T_{u,i}$ is the initial ullage temperature:

$$T_u = (\theta_w+T_b) - (\theta_w+T_b-T_{u,i})e^{\frac{-2h_3t}{Rc_p\rho}} \tag{22}$$

In addition to the stratum temperature, mixed-liquid temperature T_m is important for computing tank pressure rise:

$$\rho_m c_{p_m} T_m(\pi R^2 H) = \rho_b c_{p_b} T_b((H-\Delta)\pi R^2) + \rho_s c_{p_s} T_s(\Delta\pi R^2) \tag{23}$$

Equation (23) expresses that the mixed-liquid energy must equal the bulk and stratum energy.

Although the constant-wall-temperature model captures the general phenomenon of thermal stratification, it does not accurately mimic actual situations in which the tank is exposed to a radiation

heat flux, resulting in nonuniform wall temperatures. A model for constant wall heat flux is developed in the next section.

C. Constant-Wall-Heat-Flux Analysis

A uniform and constant wall heat flux model developed by Tellep and Harper [7] employs a modified version of the boundary-layer temperature and velocity profiles given by Eckert and Jackson [3] and Sparrow [8]. The boundary-layer mass flow entrainment for laminar and turbulent free-convection boundary layers, with constant wall heat flux and uniform bulk temperature, are given by Eqs. (24) and (25), respectively.

Laminar:

$$\dot{m}_{\text{bl}} = 2\pi R\rho\left[1.541\frac{\nu^{3/5}(g\beta q''_w/k)^{1/5}x^{4/5}}{Pr^{3/5}(\frac{4}{5}+Pr)^{1/5}}\right] \tag{24}$$

Turbulent:

$$\dot{m}_{\text{bl}} = 2\pi R\rho\left[0.286\nu^{1/7}\left(\frac{g\beta q''_w}{\rho c_p}\right)^{2/7}x^{8/7}\right] \tag{25}$$

Using Sparrow's results for laminar free convection, the growth of the stratum layer with time is given in Eq. (26), and an expression of stratum growth for turbulent boundary layers is given by Eq. (27).

Laminar:

$$\frac{\Delta(t)}{H} = 1 - \left[1 - 0.616\frac{H}{R}\frac{(Gr^*)^{1/5}}{(\frac{4}{5}+Pr)^{1/5}}\frac{1}{Pr^{3/5}}\phi\right]^5 \tag{26}$$

Turbulent:

$$\frac{\Delta(t)}{H} = 1 - \left[1 + 0.082\frac{H}{R}(Gr^*)^{2/7}\frac{1}{Pr^{2/7}}\phi\right]^{-7} \tag{27}$$

In Eqs. (26) and (27), $\phi = \nu t/H^2$. Reynolds and Satterlee [9] provide similar correlations for the growth of the stratified layer for both laminar and turbulent boundary layers with constant heat flux [Eqs. (28) and (29), respectively].

Laminar:

$$\frac{\Delta(t)}{H} = 1 - \left[1 - 0.62\frac{H}{R}(Gr^*)^{1/5}\frac{1}{Pr^{0.388}}\phi\right]^5 \tag{28}$$

Turbulent:

$$\frac{\Delta(t)}{H} = 1 - \left[1 + 0.092\frac{H}{R}\left(\frac{Gr^*}{1+0.443Pr^{2/3}}\right)^{2/7}\frac{1}{Pr^{2/3}}\phi\right]^{-7} \tag{29}$$

The value of $Gr*$ used in Eqs. (26–29) is constant for the case of constant heat flux, whereas Gr varies for the constant-wall-temperature model; at the stratum interface, θ_w is constant and Gr decreases as the height of the stratum interface moves lower. In Eqs. (26–29), the heat flux is fixed at any vertical location, but the mass flow from the boundary layer into the stratum varies with location, according to either Eq. (24) or Eq. (25).

To determine the temperature of the stratum, the energy balance of Eq. (17) is used, but modified to take into account a vertical (1-D) stratum temperature distribution as well as the heat used to vaporize the liquid. Data from a series of water experiments were used to determine the nondimensional temperature profile within the stratum, which was assumed to remain invariant with time. For the present investigation, the stratum was assumed to be isothermal, and the energy balance of Eq. (17) can be integrated to find the stratum temperature:

$$T_s = T_b + \frac{(2q''_w H + Rq''_d)t}{R\rho c_p \Delta} \tag{30}$$

Transition from a turbulent to a laminar boundary layer occurs when the stratum interface has moved below the transition distance. In the model, the Raleigh number (based on $H - \Delta$) is tracked with time. Once flow transition occurs, the reference length becomes x_{trans}. Ullage temperature is again found using an energy balance:

$$q''2\pi R(L-H) = \rho\pi R^2(L-H)c_p\frac{d\theta_u}{dt} \tag{31}$$

Similarly, Eq. (31) can be integrated to find the ullage temperature, where $T_{u,i}$ is the initial ullage temperature:

$$T_u = t_{u,i} + \frac{2q''_w t}{R\rho c_p} \tag{32}$$

Pressure rise due to the mixed fluid and ullage is determined using the first law, where subscripts m and u denote the mixed-liquid and ullage regions:

$$Q_{i\to i+1} = -2q''_w\pi RLdt = (m_m c_{p_m}\Delta T_m + m_u c_{p_u}\Delta T_u) - \pi R^2 L\Delta P \tag{33}$$

Rearranging, an expression for the tank pressure may be found:

$$P_{i+1} = \frac{2q''_w\pi RLdt + m_m c_{p_m}(T_{m,i+1} - T_{m,i}) + m_u c_{p_u}(T_{u,i+1} - t_{u,i})}{\pi R^2 L} + P_i \tag{34}$$

The models developed in Secs. II.B and II.C do not take into account the parabolic free surface of the liquid caused by rotation of the tank about its longitudinal axis, and this effect is considered in the next section.

D. Rotation Effects on Thermal Stratification

To achieve uniform heating, many upper stages are spun about their longitudinal axis. When a contained volume of liquid rotates with an angular speed ω, the free surface will form a paraboloid of revolution with height h:

$$h = \frac{(\omega R)^2}{2g} \tag{35}$$

In Eq. (35), the height that the liquid moves up the wall is $h/2$, and the vertex of the parabolic free surface is located a distance $h/2$ below the no-spin surfaces (Fig. 2). For example, fluid in a 3-m-diam tank at $g/g_0 = 10^{-4}$ and $\omega = 1$ deg /s will rise above the free surface 17 cm at the walls and the vertex will be located 17 cm below the no-spin surface.

The stratification model may be modified to include tank rotation by taking into account the increase in liquid surface area available for heating due to liquid rises along the wall, $\pi D(H + h/2)$, above the nonrotating case πDH. The resulting volume over which to spread the stratum layer will increase from a circular disk $\pi R^2\Delta$ to a parabolic disk:

$$\pi R/6h^2[(R^2 + 4h^2)^{3/2} - R^3]\Delta$$

Equation (35) neglects the effects of surface tension and wall contact angle; however, the model can be augmented to include any free-surface shape. Equation (35) also shows that for certain rotation rate and acceleration combinations, a bottomed-out or dry disk is left in the center of the tank if $h > H$.

Under rotating conditions, the liquid stratifies faster and reaches warmer stratum temperatures than when the tank is nonrotating, due to increased heating area available for the same volume of fluid. A second consequence of rotation is that the vertex of the parabola is located closer to the bottom of the tank. This means that beyond having more heating area available for the same fluid volume, there is simply less bulk liquid above the bottom center of the tank in which the propellant is drawn into the turbomachinery.

For the rotating tank, Eq. (11) is modified to take into account the paraboloid of the revolution free surface S_p:

$$\dot{m}_{\text{bl}} = S_p\rho\left(\frac{d\Delta}{dt}\right) = \frac{\pi R}{6h^2}[(R^2 + 4h^2)^{3/2} - R^3]\rho\left(\frac{d\Delta}{dt}\right) \tag{36}$$

Table 2 Comparison of percent bulk fluid remaining using Tellep and Harper [7] and Reynolds and Satterlee [9] models at a reduced-gravity ratio $g/g_0 = 10^{-4}$ at the conclusion of a 4 h coast

				Percent bulk remaining unstratified $(1 - \Delta/H) \times 100\%$		
H, m	R, m	H/R	q'', W/m^2	Tellep and Harper [7]	Reynolds and Satterlee [9]	% difference
1	1	1	10	41.2	25.5	+38
1	1	1	100	18.9	4.9	+74
2	1	2	10	36.8	48.5	−32
2	1	2	100	13.3	25.3	−90
1	2	0.5	10	65.5	31.2	+52
1	2	0.5	100	43	7.6	+82

A Bond number analysis to compare body-to-surface-tension forces indicates that for a 1.5-m-radius tank and acceleration levels greater than $10^{-6} g/g_0$, surface-tension effects can be neglected for both the LH_2 and liquid-oxygen (LOX) tanks. However, for lower acceleration levels, S_p may be replaced with a free-surface shape that includes the effects of contact angle and wall creep due to surface tension. Equations (26) and (27) can be rederived to take into account the augmented surface area available for heating and the spreading of the stratum fluid over a paraboloid free surface [rather than a disk of $S = \pi R^2 \Delta(t)$].

Laminar:

$$\frac{\Delta(t)}{H_\omega} = 1 - \left[1 - 0.616 \frac{H_\omega \pi R}{S_p} \frac{(Gr^*_\omega)^{1/5}}{(\frac{4}{5} + Pr)^{1/5}} \frac{1}{Pr^{3/5}} \phi_\omega\right]^5 \tag{37}$$

Turbulent:

$$\frac{\Delta(t)}{H_\omega} = 1 - \left[1 + 0.082 \frac{H_\omega \pi R}{S_p} (Gr^*_\omega)^{2/7} \frac{1}{Pr^{2/7}} \phi_\omega\right]^{-7} \tag{38}$$

In Eqs. (37) and (38), the new modified Grashof numbers Gr^*_ω are evaluated at the initial fill level plus the increased height up the tank wall that the liquid travels due to rotation, $H_\omega = H + h/2$ and $\phi_\omega = \nu t / H^2_\omega$. Stratum temperature relations are the same as before, but H is now replaced with H_ω.

III. Results and Discussion

Although Eqs. (26) and (27) look similar to Eqs. (28) and (29), the models define $Gr*$ in a different manner. Reynolds and Satterlee [9] use $Gr*$ based on tank radius R, and Tellep and Harper [7] use $Gr*$ based on initial bulk fill level H. The models assume that the warm fluid exiting the boundary layer immediately forms a uniform thickness disk of the stratified fluid; radial inflow effects are neglected. For large H/R ratios, flow in the radial direction occurs quickly compared with vertical boundary-layer flow, and the assumption that the warm boundary-layer fluid quickly takes a disk shape is more valid. In contrast, for small H/R, the time for the flow to travel radially inward from the boundary layer and meet in the center of the tank may not even occur during the mission time [5]. Most current upper-stage vehicles have $H/R < 1$ at the start of the coast phase (typically, 10–20% of the propellant remains for the final insertion burn [1,2]). The two models yield very different results over a range of H/R values, and the reader is cautioned to understand the definition of $Gr*$ used in each, although trends with acceleration level, heat flux, and bulk fill level track similarly between the two models. Table 2 summarizes the amount of bulk fluid remaining unstratified $(1 - \Delta/H)$ at the conclusion of a 4 h coast for heat fluxes of 10 and 100 W/m^2.

Because the $Gr*$ used in relations developed for flat plates for which the plates' vertical length is the relevant length, the Tellep and Harper [7] model is used hereafter because of its use of the vertical tank fill height as the reference length.

Figure 3 shows the results of the stratification model developed previously for a constant tank-wall heat flux of 5 and 10 W/m^2 at reduced-gravity ratios of $g/g_0 = 10^{-2}$ and 10^{-4}, and it includes the effect of boundary-layer transition.

The plots of Fig. 3 show the fraction of cold bulk liquid remaining (upper plots) and the stratum temperatures (lower plots) versus time for LH_2 (left plots) and LOX (right plots) at heat fluxes of 5 and 10 W/m^2 and reduced-gravity ratios of 10^{-2} and 10^{-4} for a 4 h coast. For LH_2 at 5 and 10 W/m^2 and $g/g_0 = 10^{-4}$, the boundary layers are always laminar and the stratification proceeds more slowly than the same heat fluxes at $g/g_0 = 10^{-2}$, where the boundary layers

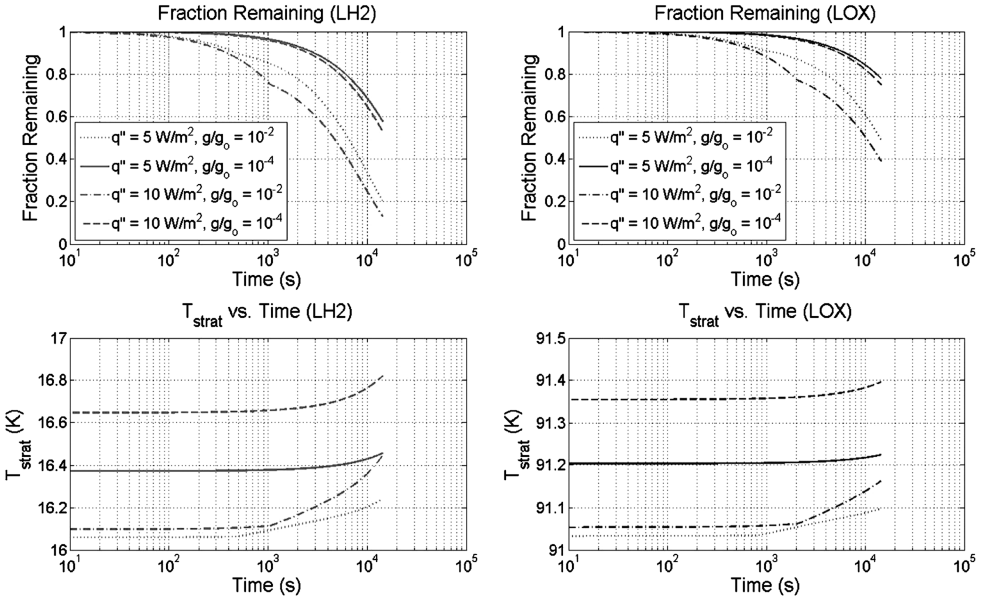

Fig. 3 Plots of percent bulk remaining and stratum temperatures vs time for LH_2 and LOX at heat fluxes of 5 and 10 W/m^2 and reduced-gravity ratios of $g/g_0 = 10^{-2}$ and 10^{-4} for a 4 h coast duration.

begin turbulent and then transition to laminar. This transition can be seen by the abrupt change in slope in the fraction of remaining bulk curves for both LH_2 and LOX at $g/g_0 = 10^{-2}$. The model shows that stratification occurs faster for turbulent boundary layers at higher acceleration levels and higher heat fluxes. The lower plots show the temperature of the stratum with time. The stratum temperature has an initial jump at $t = 0^+$, because the warm boundary-layer fluid, which is taken as fully developed at $t = 0$, is immediately dumped into the stratum layer. The plots show that although stratification proceeds more rapidly at high acceleration levels and for turbulent boundary layers, the temperature of the stratified layer is higher at lower acceleration levels when the boundary layers are laminar. To summarize, consider the 10 W/m^2 cases at $g/g_0 = 10^{-2}$ and 10^{-4}. In this case, the 10^{-2} acceleration stratifies more rapidly, but the stratum does not become as warm as in the 10^{-4} case.

Figure 4 shows an example of the effects of rotation on stratification for LH_2 and LOX at heat flux of 5 W/m^2, $g/g_0 = 10^{-4}$, and spin rates of $\omega = 0$ and 1 deg /s.

The curves that show the percentage of bulk remaining with rotation are normalized to the equivalent no-spin liquid fill level for comparison. The plot shows that for $\omega = 1$ deg /s and $g/g_0 = 10^{-4}$, the bulk fluid stratifies faster, however, the stratum temperature is cooler than in the no-spin case. This effect is due to decreased H_ω/Δ values when spin is included.

Within the range of conditions given in Table 1, spin always causes an increase in the stratified-layer thickness. For a fixed spin rate, as the acceleration level decreases, stratification increases, due to the increased heating area between the fluid and tank walls. However, the stratum temperatures may be cooler or warmer than in the equivalent no-spin case. The stratum temperatures initially decrease with spin rate until a critical value of spin rate is reached, and then the stratum temperature increases with further increasing spin rate. The critical spin rate corresponds to the minimization of H_ω/Δ. For a given fill level and radius, the critical spin rate increases as acceleration level increases. For a given fill level and gravity level, increasing the tank radius decreases the critical spin rate but cools the stratum more. This critical-spin-rate effect can be further understood by considering that when spinning occurs, there is indeed more wall surface area available for heating the fluid, due to the parabolic dishing effect; however, at the same time, the area over which the warm fluid may now be spread is no longer a cylindrical disk, but is now the disk associated with the paraboloid of revolution. Above the critical spin rate, the increased surface area for heating dominates the increased stratum-layer volume, and the stratum temperature is warmer than in the equivalent no-spin case. In contrast, for spin rates below the critical value, the increased wall-heating area is more than offset by the increased stratum-layer volume, and the resulting stratum layer is slightly cooler than in the equivalent no-spin case. Table 3 summarizes the results of stratification for a 3 m square-cylinder tank filled with 20% LH_2 and wall heat flux of 10 W/m^2 at 10^{-2} and 10^{-4} gravity levels for various spin rates.

Table 3 Summary of LH_2 stratification for $R = 1.5$ m, $H = 0.6$ m, and $q'' = 10$ W/m^2

ω, deg /s	g/g_0	Percent bulk remaining unstratified $(1 - \Delta/H_\omega) \times 100\%$	$\theta_s = Ts - Tb$, K
0	10^{-2}	37	0.3
1	10^{-2}	36.5	0.305
5	10^{-2}	32	0.31
0	10^{-4}	73	0.73
1	10^{-4}	64	0.68
1.5	10^{-4}	56	0.74

Most coast phases do not have a constant acceleration profile, and for this scenario, the governing equations may be numerically integrated for an arbitrary acceleration profile. As an example, consider three acceleration profiles. Two of these profiles are constant over time and are the minimum [low acceleration (LA)] and maximum [high acceleration (HA)] of a time-varying profile (variable acceleration). In general, any initial burn will cause the stratification rates to increase relative to a low-acceleration case. Over a prescribed period of time, the resulting larger stratification rates will lead to cooler stratum layers. As a result, for a certain period of time, mixed-fluid temperatures will then be cooler and tank pressures will be lower for the variable-acceleration case than with the HA case. After some period of time, the increase in θ_s dominates over the increased stratum thickness development; as a result, mixed-fluid temperatures and tank pressures rise above the HA case and tend toward the LA case, in which θ_s, θ_m, and tank pressures are always larger because of slower stratum-layer thickness development.

The analytical models assume steady-state rotation and a fully established free-convection boundary layer; however, these time scales may be a significant fraction of the total coast time. For example, it may only take seconds for the boundary layer to reach steady state at $g/g_0 = 1$, but it could take over an hour to reach steady state when the axial acceleration is lower than $g/g_0 = 10^{-3}$. Low acceleration also increases the steady-state time scale for a rotating

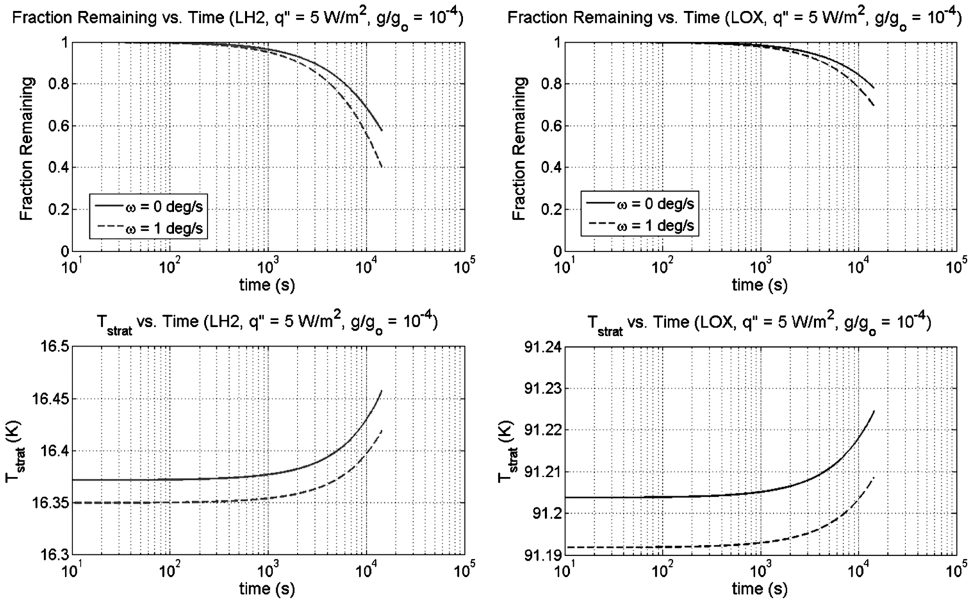

Fig. 4 Example of the effect of rotation on thermal stratification and stratum temperature for LH_2 and LOX at heat flux of 5 W/m^2, reduced gravity of $g/g_0 = 10^{-4}$, and spin rates of $\omega = 0$ and 1 deg /s.

liquid to achieve solid body rotation, which may also be on the order of hours. Another feature not captured by the analytical models is the presence of secondary flows resulting from the recirculation of boundary-layer exit fluid flowing radially inward through the stratum and then being forced back down the axis of the tank. As the fluid travels down the axis of the tank it is cooled by cold bulk and may be once again be entrained by the boundary layer. These effects are beyond the scope of the simplified analytical models presented here; however, to capture such phenomena, unsteady computational fluid dynamics (CFD) models have been developed to assess the importance of these effects, which are discussed in [5]. Nonetheless, the analytical models provide quick estimates of stratification and accurately predict trends with rotation rate, heat flux, axial acceleration level, and tank geometry.

Many stratification models take into account energy transfer to the ullage but neglect mass transfer through evaporation. To check this assumption, the amount of evaporation of LOX into a helium ullage was estimated over a 4 h period using a 1-D Stefan problem for a closed container. The ullage was taken to be initially composed of 100% helium, the ullage pressure was 207 kPa, the LOX temperature was 91 K, and the 4 m square-cylinder tank was filled to a 30% fill level containing 17,200 kg of LOX. The concentration of the oxygen/helium mixture varies with time, and at the interface, the partial pressure on the gas side of the interface equals the saturation pressure associated with the temperature of LOX. The interface height also decreases with time due to evaporation. The binary diffusion coefficient for oxygen into helium at these conditions is 4.76×10^{-6} m^2/s. The mass diffusion per unit area is found to be 1.13×10^{-5} $kg/s \cdot m^2$ and the evaporation mass flow rate is 1.68×10^{-4} kg/s, which results in 2.4 kg of LOX diffused in helium/oxygen and a reduction in the liquid free-surface height of $\Delta H = 0.17$ mm at the conclusion of the 4 h coast. An energy balance across the liquid-gas interface predicts evaporative cooling of the LOX by 0.018 K. As both of these values are small, neglecting evaporation is reasonable; however, it should be noted that for longer periods of time (i.e., weeks or months) of cryogenic storage, these effects become significant.

IV. Conclusions

To ensure proper operation of upper-stage engine turbomachinery after an orbital transfer coast, accurate modeling of the thermodynamic state of the propellants is needed. This work reviewed and then extended existing analytical stratification models to include and assess the impact of the spinning of a tank about its longitudinal axis as well as boundary-layer transition that commonly occurs with the tank fills levels and acceleration environments of the upper stages of a launch vehicle during orbital transition coasts. For typical upper-stage coast scenarios, boundary layers can begin laminar and transition to turbulent as the tank walls warm up due to solar heating. As the stratum layer begins to propagate, the boundary-layer run length is reduced and the turbulent boundary can transition back to laminar. The analytical models developed in this work are capable of handling boundary-layer transition as well as the effects of tank rotation about its longitudinal axis. The following conclusions have been drawn:

1) Thermal stratification increases as the acceleration level is increased and as the wall heating is increased. Turbulent boundary layers lead to faster stratification times, but the temperature of the stratum may be lower than in a laminar boundary-layer situation; accurately modeling the boundary-layer type is essential to predicting the stratification time and final stratum temperature.

2) The impact of the spin at low acceleration levels is a significant parabolic free-surface shape that leads to an increased area available for heating of the propellant for the same volume of bulk fluid.

3) The consequence of spin is that stratification times are shorter and the stratum temperatures can be either warmer or cooler, as compared with the zero-spin case under the same incident heat flux loads.

4) The ullage pressure rise associated with a thermally stratified tank is greater than the pressure rise associated with the cryogenic fluid mixed at uniform temperature.

Acknowledgments

This work was made possible by Analex agreement numbers 05-001 and 06-001. The authors also wish to thank Mike Campbell, Sukhdeep Chase, Martin Margulies, Cindy Fortenberry, and Xiaoyi Li of the NASA John F. Kennedy Space Center Launch Services Program and Analex Corporation for their technical input, advice, and highly beneficial suggestions for improvement to this work.

References

[1] Schallhorn, P., Campbell, D. M., Chase, S., Piquero, J., Fortenberry, C., Li, X., and Grob, L., "Upper Stage Tank Thermodynamic Modelling Using SINDA/FLUINT," 2006 AIAA Joint Propulsion Conference, Sacramento, CA, AIAA Paper 2006-5051, July 2006.

[2] Berglund, M. D., Bassett, C. E., Kelso, J. M., Mishic, J., and Schrage, D., "The Boeing Delta IV Launch Vehicle—Pulse-Settling Approach for Second-Stage Hydrogen Propellant Management," *Acta Astronautica*, Vol. 61, Nos. 1–6, June–Aug. 2007, pp. 416–424. doi:10.1016/j.actaastro.2007.01.048

[3] Eckert, E. R. G., and Jackson, T. W., "Analysis of Turbulent Free-Convection Boundary Layer on a Flat Plate," Lewis Flight Propulsion Lab., Cleveland, OH, July 1950.

[4] Bailey, T., VandeKoppel, R., Skartvedt, D., and Jefferson, T., "Cryogenic Propellant Stratification Analysis and Test Data Correlation," *AIAA Journal*, Vol. 1, No. 7, 1963, pp. 1657–1659. doi:10.2514/3.1875

[5] Kirk, D. R., and Oliveira, J., "Modeling of Upper-Stage Cryogenic Propellant Stratification in a Rotating, Reduced Gravity Environment," AIAA Joint Propulsion Conference, Sacramento, CA, AIAA Paper 2006-5059, 2006.

[6] Oliveira, J. M., and Kirk, D. R., "The Effect of an Isogrid on Cryogenic Propellant Behavior and Thermal Stratification," AIAA Joint Propulsion Conference, Cincinnati, OH, AIAA Paper 2007-5497, 2007.

[7] Tellep, D. M., and Harper, E. Y., "Approximate Analysis of Propellant Stratification," *AIAA Journal*, Vol. 1, No. 8, 1963, pp. 1954–1956. doi:10.2514/3.1977;

[8] Sparrow, E. M., "Laminar Free Convection on a Vertical Plate with Prescribed Nonuniform Wall Heat Flux," NACA TN 3508, July 1955.

[9] Reynolds, W. C., and Satterlee, H. M., "Liquid Propellant Behavior at Low and Zero g," *The Dynamic Behavior of Liquids in Moving Containers*, NASA, Rept. NASA SP-106, 1965, p. 387.

G. Palmer
Associate Editor